J. Fluid Mech. (1981), *vol.* 108, *pp.* 401–421
Printed in Great Britain

The nonlinear behaviour of a constant vorticity layer at a wall

By D. I. PULLIN

Department of Mechanical Engineering, University of Melbourne,
Parkville, 3052 Victoria, Australia

(Received 25 March 1980 and in revised form 21 October 1980)

The so-called 'water-bag' method is used to study the behaviour of a two-dimensional inviscid layer of constant vorticity ω and of mean thickness δ adjacent to a wall with slip at the wall. A nonlinear initial-value equation is derived which describes the motion of the material interface separating the rotational fluid within the layer from the irrotational free stream, for the case where this interface is subject to streamwise cyclic disturbances to its undisturbed shape. A linearized solution to this equation shows that a sinusoidal disturbance of wavelength λ propagates as one mode of a neutrally stable Kelvin–Helmholtz wave with velocity $\omega\lambda[1-\exp(-4\pi\delta/\lambda)]/4\pi$ relative to the fluid at infinity. Numerical solutions of the full nonlinear equation for a range of wavelengths and finite disturbance amplitudes indicate different behaviour. For sufficiently large amplitude the interface valleys evolve into long re-entrant wedges of irrotational fluid which are 'entrained' into the layer and which are separated from the free stream by lobes or bulges of rotational fluid. This single-mode nonlinear interfacial distortion could be generated over a broad wavelength range with no indication of preferential scaling based on δ. It is suggested that the interface behaviour bears distinct resemblance to flow features observed at the interface between turbulent and non-turbulent fluid in recent smoke-in-air flow-visualization studies of the outer part of a constant pressure turbulent boundary layer. The calculated rotational fluid lobe velocities, which are not very different from the equivalent linearized wave velocities, are found to be in reasonable agreement with the few existing measurements of the velocity of bulges at the turbulent–nonturbulent fluid interface, while the computed velocity field in the lobe is in qualitative agreement with the general flow pattern observed in experiments. In the absence of a preferred scale or range of scales for the development of the interfacial distortion, however, it is concluded that the present results cannot be interpreted as supporting the hypothesis of the presence of large-scale coherent motions in the outer part of the layer.

1. Introduction

It is widely recognized that the dynamics of unsteady two-dimensional vortex interactions are of considerable relevance to the study of many plane high-Reynolds-number flows in which free circulation can be seen to play a significant role (for a recent survey of the subject see Saffman & Baker 1979). For a particular flow the usual approach has been to model the dominant features of the unsteady circulation distribution either by arrays of point vortices (Acton 1976), where a finite-vorticity

approximation is required, or by vortex sheets (e.g. Fink & Soh 1978), where the thin-shear-layer approximation is thought to be adequate. The calculated (on a digital computer) time evolution of the circulation system may then be studied as a means of identifying the key structural features of the flow development. The principal motivation for such studies is the belief that the behaviour of persistent organized structures which have been observed experimentally in many turbulent flows may be explained as a direct consequence of the overall nonlinear inviscid vortical interaction.

Both the point-vortex method, or hybrid variations such as the 'cloud-in-cell' method (Christiansen 1973; Christiansen & Zabusky 1973; Roberts & Christiansen 1972), and the vortex-sheet approach may be regarded as attempts to solve Euler's equation in the form of the nonlinear unsteady inviscid vorticity equation in two dimensions. For different reasons both methods contain inherent theoretical difficulties which are probably related to their numerical performance. Saffman & Baker (1979) point out that a moving array of point vortices is at best a weak solution of Euler's equation. Moreover, this approach cannot be readily studied analytically to determine for example its behaviour in the linearized approximation for given initial and boundary conditions. There is increasing evidence (see Moore 1979) that the Birkhoff–Rott vortex-sheet equation (Birkhoff 1962; Rott 1956) does not constitute a well-posed initial-value problem at all in many instances. The result is that the vortex-sheet model may be physically realistic only in situations in which it is undergoing continuous lateral stretching in the plane of the two-dimensional motion, otherwise exhibiting non-physical pathologically unstable behaviour. An attempt by Moore (1978) to extend the model to a vortex layer of thickness which is everywhere small compared to the local radius of curvature does not remedy matters since the spurious short-wave instability is not eliminated.

It is clearly desirable to proceed beyond the vortex sheet and point-vortex approaches to consider the dynamics of properly continuous and finite-vorticity distributions. For inviscid flow the simplest and mathematically most convenient initial distribution is that of constant vorticity ω within several regions R_j since in this case for two-dimensional flow (as will be seen) the entire fluid motion can be reduced to the motion of the curves C_j bounding the R_j. Such an approach has been termed the water-bag method, the ω = constant 'water bags' being the R_j moving in the irrotational 'dry' surroundings. This method has been developed by several workers but most completely by Deem & Zabusky (1978*a*, *b*) and Zabusky, Hughes & Roberts (1979). These authors have used a real-variable formulation of the technique to study the nonlinear motion of isolated and interacting closed uniform vortices. A similar application has been given by Seo, Joynt & Llewelyn (1979). The model is related by analogy to a similar model in plasma physics (see Berk, Nielsen & Roberts 1970) of the unsteady one-dimensional Vlasov equation (in fluid mechanics read two-dimensional vorticity equation) in phase space (physical space) for the plasma distribution function (vorticity) with long-range nonlinear coulombic (vortical) interactions. The common feature of these and other similar nonlinear systems that can be treated using the water-bag approach is the existence of a Hamiltonian formulation of the equations of motion which is only possible in fluid mechanics for two-dimensional inviscid flow.

In the present work we apply the water-bag model to the nonlinear inviscid stability of an infinite layer of constant vorticity fluid adjacent to a solid wall, with slip at the wall. This problem is of interest firstly since there exists a linearized analysis (see

Rayleigh 1887 and the appendix) which indicates well-behaved neutral stability and which may serve as an analytical framework for interpreting the nonlinear results. Secondly, the model may have some at least qualitative relevance to the behaviour of the outer part of a fully developed constant pressure turbulent boundary layer, in particular to the formation of large-scale bulges at the turbulent–non-turbulent fluid interface observed by Kovasznay, Kibens & Blackwelder (1970), Falco (1977), Brown & Thomas (1977) and other workers. It is true that the vorticity derived from the mean-velocity profile is not constant over the outer part of the turbulent boundary layer. Kovasznay *et al.*, however, using conditional averaging techniques based on the intermittency concept to distinguish between turbulent and non-turbulent fluid, found that the mean vorticity of the turbulent fluid within the outer bulges *was* nearly constant. Furthermore, as will be seen, the unsteady constant vorticity model contains natural material boundaries (the C_j) which may be identified with the experimentally observed sharp interface between the vortical turbulent fluid and the irrotational free-stream fluid. The application of the constant-vorticity inviscid model to boundary-layer behaviour has some precedent in the work of Perry & Fairlie (1975) who successfully applied the model to the steady flow formation of a separation–reattachment bubble within an adverse pressure gradient turbulent boundary layer.

More serious than the constant vorticity assumption is the neglect in the present model of three-dimensional fluctuations which many workers feel are crucial to an understanding of all aspects of turbulent near-wall flows. Hence, even if the instantaneous vorticity were initially constant, it could not remain so owing to three-dimensional vortex stretching. But, while it seems certain that a fully three-dimensional model, perhaps of the type proposed by Perry, Lim & Chong (1980) (see also the extensive three-dimensional calculations of Leonard 1980), is necessary to explain the observed structure in the logarithmic mean-velocity profile region and in the viscous sublayer, it is less clear that three-dimensional motions are an essential ingredient in the dynamics of the outer part of the layer, particularly in respect of any large-scale, possibly coherent, motions. It will be presently seen that flow features bearing a distinct resemblance to behaviour observed in boundary-layer flow-visualization studies may result from a purely two-dimensional nonlinear vortical interaction.

In the following a complex variable formulation of the water-bag method is given in §2. The method is applied in §3 to an infinite vortical layer at a wall with cyclic initial conditions on the material interface between vortical and non-vortical fluid, resulting in a nonlinear initial-value problem for the motion of the interface. A numerical model of the nonlinear equation is subsequently formulated, while the results of the numerical calculations are described and discussed in §4. An analytical solution of the linearized equation is given in the appendix.

2. General theory

For simplicity we shall here consider the motion from time $t = t_0$ of a single simply connected region R of fluid of constant vorticity ω due to both its own self-induction and to the influence of an external applied velocity field. This region is assumed to be bounded by a closed piecewise continuous curve $C(t)$, the sense of which will be taken to be in the clockwise direction around R. The fluid outside R is assumed to be irrotational and the entire motion is assumed to be two-dimensional motion of an inviscid

fluid. We work in the complex $Z = X + iY$ plane. At any $t \geqslant t_0$, $C(t)$ will be described by the complex single-valued function $z(s,t) = x(s,t) + iy(s,t)$, where s is a parameter (not necessarily arc length) which may be taken to increase along $C(t)$ clockwise. Since outside R the fluid is irrotational, there exists a complex potential $W = \phi + i\psi$ which by virtue of ω = constant may be written as

$$W(Z) = \frac{\omega}{2\pi i} \iint_R \log(Z - Z')\, dX'\, dY' + W_e, \tag{1}$$

where $Z = X' + iY'$ is a point in R. In (1) the first term is the complex potential due to the vortical fluid in R while W_e is that due to external influences. The complex velocity $dW/dZ = u - iv$ is then

$$\frac{dW}{dZ} = \frac{\omega}{2\pi i} \iint_R \frac{dX'\, dY'}{Z - Z'} + \frac{dW_e}{dZ}. \tag{2}$$

Applying the complex Green's theorem for C clockwise

$$\iint_R (\partial F(Z, Z')/\partial Z')\, dX'\, dY' = -\tfrac{1}{2} i \oint_C F(Z, z')\, d\bar{z}',$$

to the double integral in (2) yields

$$\frac{dW}{dZ} = \frac{\omega}{4\pi} \oint_C \log(Z - z')\, d\bar{z}' + \frac{dW_e}{dZ}. \tag{3}$$

In equation (3) with Z fixed the log is defined as any branch which remains single-valued as z' traverses C.

Now, whatever the motion of R for $t \geqslant t_0$ as a result of the overall velocity field, the vorticity at every point within R must remain constant and equal to ω by Helmholtz's theorem for inviscid two-dimensional flow. Moreover, C must remain a material curve which always delineates a boundary or interface between vortical and irrotational fluid. It is also true that the complex velocity of a particular particle on C at t may be written

$$u - iv = \frac{\partial \bar{z}(s,t)}{\partial t}, \tag{4}$$

where we have adopted the convention that s remains constant in time on a particular particle comprising C so that this quantity acts as a particle label. In fact s will presently be seen to be a purely formal parameter used in practice only to define the initial conditions. We now allow $Z \to z(s,t)$ on C in (3) and equate the right-hand side of (4) to the result, leading to an initial-value problem for the motion of C,

$$\frac{\partial \bar{z}}{\partial t} = \frac{\omega}{4\pi} \oint_C \log(z - z')\, d\bar{z}' + \frac{dW_e}{dz}, \tag{5}$$

with initial condition $z(s, 0)$.

Although we shall subsequently use (5) directly, it is convenient here to develop the equation into a simpler form. This can be achieved by transforming the integration with respect to $\bar{z}'$ to that with respect to s' and integrating the result by parts to give

$$\frac{\partial \bar{z}}{\partial t} = -\frac{\omega}{4\pi} \oint_C \frac{\bar{z} - \bar{z}'}{z - z'}\, dz' + \frac{dW_e}{dz}. \tag{6}$$

Equation (6) is relatively simple for the purposes of numerical integration since as $z \to z'$ on C the integrand takes the finite value $d\bar{z}/dz = \exp(-2i\theta)$, where θ is the tangent angle of C to the X direction at z.

Equation (5) or (6) is a mixed Eulerian–Lagrangian description of the motion of R in terms of the motion of C. The equations may be shown to preserve in time the constancy of the various integral invariants of the vorticity field (see Batchelor 1967, cha. 7). In addition, for several interacting regions it may be shown that the number of regions and the number and topology of the curves bounding these regions also remain invariant with time. The equations may be viewed as a generalization of the Birkhoff–Rott vortex-sheet equation and may be reduced to this equation when R is compressed into an infinitesimally thin region with $\omega \to \infty$ and area $\to 0$ such that $\omega \times$ area = circulation remains finite. One further point which should be noted is that the right-hand side of (6) with z replaced by Z may be interpreted as the complex velocity $u - iv$ even if Z lies within R. This may be demonstrated by deforming C for Z in R by the introduction of a cut joining Z to any part of the original boundary, required so as to make $\log(Z - z')$ a single-valued function for application of the complex Green's theorem. The contribution to the integral along both sides of the cut in (6) (but not in (5)) and around a small circle surrounding Z in R may then be shown to vanish. In this case, however, $u - iv$ is no longer an analytic function of Z alone. In the corresponding expression for W, $\psi = \mathrm{Im}(W)$ is still valid but the real part of W has no meaning as a velocity potential.

3. Vortical layer at a wall

3.1. *Formulation of initial-value problem*

Here we shall apply (5) to the present case of a vortical layer of constant strength at a wall with slip at the wall. In the Z plane, the wall is given by $Y = 0, \infty > X > -\infty$. In the unperturbed state, the vortical layer of constant strength ω and thickness δ lies in $\delta \geqslant Y \geqslant 0$ extending to infinity in the $+X$ and $-X$ directions. The fluid above the layer is irrotational. We shall work in a frame of reference at rest with respect to the fluid at infinity so that the unperturbed velocity field is

$$u = 0, \quad v = 0, \quad \infty \geqslant Y \geqslant \delta, \tag{7a}$$

$$u = \omega(\delta - Y), \quad v = 0, \quad \delta \geqslant Y \geqslant 0. \tag{7b}$$

We shall take $\omega < 0$ so that the fluid speed at $Y = 0$ is in the negative X direction. To relate the model to a possible boundary-layer flow, we need to introduce a further effective slip velocity U_1 representing the velocity change over the inner part of the layer (compressed here onto a vortex sheet at $Y = 0$) so that the free-stream speed relative to an observer at rest with respect to the wall is

$$U_0 = |\omega|\delta + U_1. \tag{8}$$

Note that this slip velocity would play no part in the model dynamics since the vortex sheet always remains attached to the wall. An alternative to (8) is to relate $|\omega|\delta$ directly to mean-flow properties other than U_0, in particular to the friction velocity u_*. Since there is some experimental justification for such a relationship (Kovasznay *et al.* 1970), it is the procedure followed in §4.2.

We consider the evolution of periodic disturbances in the vortical boundary of fixed wavelength λ in the X direction. Let the basic cycle of the disturbance on which we shall fix our attention be a single wavelength in $x_0 \geqslant X > x_0 + \lambda$, where $x_0 = x_0(t)$

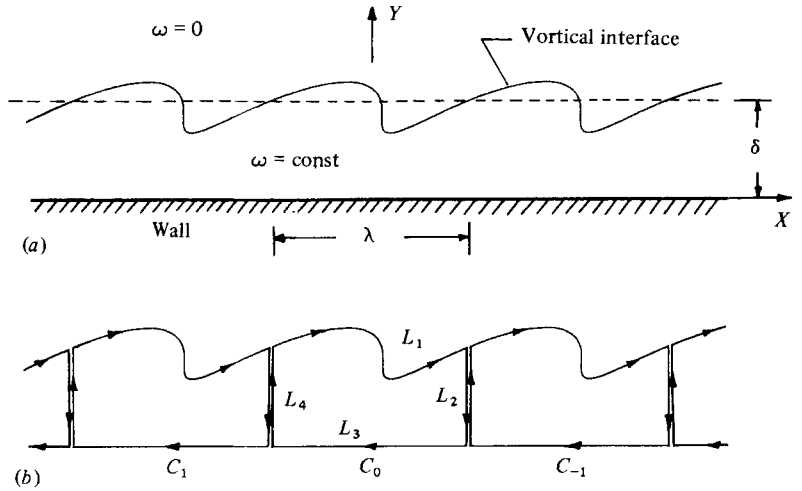

FIGURE 1. (*a*) Periodic disturbance of interface between fluid of constant vorticity ω adjacent to a wall and irrotational fluid at rest at infinity. (*b*) Rotational fluid region bounded by curves C_j, $j = -\infty, \infty$.

is to be determined. Now consider $2M+1$ cycles comprising the basic cycle together with M repeated cycles in each of the $+$ and $-X$ directions. Denote by C_j, $j = -M, \ldots, M$, the curve in the clockwise direction surrounding the vorticity contained between the jth cycle of the boundary and the wall, and bounded at $x = x_0 + j\lambda$, $x_0 + (j+1)\lambda$ by vertical lines. The curves C_{-1}, C_0 and C_1 are shown in figure 1 (*b*). Then, applying (5), the equation of motion of points on the interface in the basic cycle is

$$\frac{\partial \bar{z}}{\partial t} = \underset{M\to\infty}{\frac{\omega}{4\pi}} \left\{ \sum_{j=-M}^{M} \oint_{C_j} \log(z-z')\,d\bar{z}' + \oint_{C_j} \log(z-\bar{z}')\,dz' \right\}, \tag{9}$$

where the second integral represents the complex velocity due to the image of the vorticity field in the wall, introduced so as to satisfy the boundary condition of zero normal velocity at the wall. Now C_j is transformed to C_0 surrounding the basic cycle of vorticity in each term of (9) by replacing z' by $z' + j\lambda$, $j = -M, \ldots + M$. Manipulating the result of this transformation, and utilizing a well-known product definition of the sine function in the $M \to \infty$ limit leads to

$$\frac{\partial \bar{z}}{\partial t} = \frac{\omega}{4\pi} \left\{ \oint_{C_0} \log\left[\sin\left(\frac{\pi}{\lambda}(z-z')\right)\right] d\bar{z}' + \oint_{C_0} \log\left[\sin\left(\frac{\pi}{\lambda}(z-\bar{z}')\right)\right] dz' \right\}. \tag{10}$$

We now break C_0 up into segments L_1, L_2, L_3 and L_4 as shown in figure 1 (*b*), where L_1 is the vortical interface and L_2, L_3 and L_4 are straight sections. The contributions to the integrals in (10) along L_2, L_3 and L_4 may be evaluated with contour integration to yield the nonlinear initial-value equation for $z(s,t)$ (including $z_0 = x_0 + iy_0$) representing the evolution of general periodic disturbances in the vortical interface,†

$$\frac{\partial \bar{z}}{\partial t} = \frac{\omega}{4\pi} \left\{ \int_{L_1} \log\left[\sin\left(\frac{\pi}{\lambda}(z-z')\right)\right] d\bar{z}' + \int_{L_1} \log\left[\sin\left(\frac{\pi}{\lambda}(z-\bar{z}')\right)\right] dz' \right\} + \frac{\omega}{2}\{i(z-x_0) + K\lambda\}, \tag{11}$$

† Note that we do not need to consider directly the motion of L_2–L_4 since these lines lie within the vortical layer. Hence, for the purposes of evaluating the velocity field on L_1, L_2, L_3 and L_4 may be taken as instantaneously straight.

where $K = \log(2)/\pi - i$ is a complex constant. The initial conditions on (11) are given as $z(s, 0)$ at $t = 0$. Equation (11) is valid for finite δ. An equation valid for infinite δ or equivalently for an isolated vortical interface, in a framework at rest with respect to the irrotational fluid at infinity, may be obtained by replacing z by $z - i\delta$ in (11) and taking the limit of the result as $\delta/\lambda \to \infty$, giving

$$\frac{\partial \bar{z}}{\partial t} = \frac{\omega}{4\pi} \int_{L_1} \log\left[\sin\left(\frac{\pi}{\lambda}(z - z')\right)\right] d\bar{z}' + \frac{\omega}{4}\{i(z - \bar{z}_0) + K\lambda\}. \tag{12}$$

In obtaining (12) it has been assumed that X axis is initially the mean level of L_1 so that by conservation of circulation

$$\int_{L_1} y\,dx = 0 \quad \text{for all} \quad t > 0.$$

Equations (11) and (12) have been derived on the tacit assumption that L_1 does not become sufficiently distorted so as to extend outside of the basic wavelength range $x_0 \geqslant X > x_0 + \lambda$. It may be nevertheless shown that these equations remain valid in the event of such distortions provided one chooses the branch of

$$\log[\sin(\pi/\lambda(z - z'))]$$

to be used in the calculations carefully. The explicit details are not given here.

The linearized stability of the constant vorticity layer was treated by Rayleigh (1887). From the general theory of inviscid stability of plane parallel flows it is known the layer must be stable to small disturbances, since the unperturbed velocity profile does not contain a point of inflection. The specific result, which may also be obtained directly from a linearized solution of (11) (see the appendix), is that a sinusoidal disturbance of wavelength λ on the interface moves as a stable dispersive Kelvin–Helmholtz wave travelling in the same direction relative to the fluid at infinity as is the wall, with phase velocity

$$c = \frac{\omega\lambda}{4\pi}(1 - e^{-4\pi\delta/\lambda}). \tag{13}$$

This result shows that short waves such that $\delta/\lambda \gg 1$ move with the free stream while long waves, $\delta/\lambda \to 0$, move at a velocity which is asymptotically $\omega\delta$ with respect to the free stream. The wave period is then

$$t_w = -\frac{4\pi}{\omega}(1 - e^{-4\pi\delta/\lambda})^{-1}. \tag{14}$$

Material particles on the interface move in periodic trajectories with period t_w so that this quantity is the natural time scale associated with wavelength λ. Wavelike behaviour of a vortical interface has also been studied by Deem & Zabusky (1978*a*, *b*) who have obtained a class of nonlinear dispersive wave solutions (so-called 'V states') of the Euler equations for rotating and translating finite-area uniform vortices. By analogy it is possible that finite-amplitude nonlinear progressive-wave-like solutions exist for the present configuration (for which the linearized solution is the small-amplitude limit) but this aspect of the problem has not been pursued in the present work.

3.2. *Numerical solution of the nonlinear equation*

Introducing dimensionless variables $\zeta = \xi + i\eta$ and τ given by

$$\zeta = z/\lambda, \quad \tau = -\omega t \tag{15}$$

into (11) yields

$$\frac{\partial \bar{\zeta}}{\partial \tau} = -\frac{1}{4\pi}\left\{\int_{L_1} \log\left[\sin\left(\pi(\zeta - \zeta')\right)\right] d\bar{\zeta}' + \int_{L_1} \log\left[\sin\left(\pi(\zeta - \bar{\zeta}')\right)\right] d\zeta'\right\} - \tfrac{1}{2}\{i(\zeta - \xi_0) + K\}, \tag{16}$$

where the integration along L_1 extends from $\zeta_0 = \xi_0 + i\eta_0$ to $\zeta_{N+1} = \zeta_0 + 1$. Now the integrand in the first term of (16) has singularities at $\zeta' = \zeta \pm k, k = 0, 1, 2, \ldots$, of which only $\zeta' = \zeta$ lies within the integration range except where $\zeta = \zeta_0$ or $\zeta = \zeta_{N+1}$, in which case a second singularity at $\zeta = \zeta_{N+1}$ or ζ_0 respectively is introduced. Thus when ζ lies near (but not at) either ζ_0 or ζ_{N+1} the singularity at $\zeta = \zeta + 1$ or $\zeta - 1$ respectively generates a large (but finite) integrand near the other end point, which is unsuitable for numerical quadrature. To alleviate this problem we add and subtract

$$\log\left[\pi(\zeta_s - \zeta)\right]$$

to the integrand of the first term in (17), where we arbitrary choose $\zeta_s = \zeta - 1$ if $\xi > \xi_0 + \frac{1}{2}$ and $\zeta_s = \zeta + 1$ if $\xi \leqslant \xi_0 + \frac{1}{2}$. Integrating the result by parts, which eliminates the singularity at $\zeta = \zeta'$, we obtain

$$\begin{aligned}\frac{\partial \bar{\zeta}}{\partial \tau} = &-\frac{1}{4\pi}\{[F(\zeta, \zeta_0) - G(\zeta_s, \zeta_0)] - [F(\zeta, \zeta_{N+1}) - G(\zeta_s, \zeta_{N+1})] + F(\zeta, \bar{\zeta}_0) - F(\zeta, \bar{\zeta}_{N+1})\} \\ &+ \frac{1}{4}\int_{\zeta_0}^{\zeta_{N+1}} (\bar{\zeta} - \bar{\zeta}')\left\{\cot\left(\pi(\zeta - \zeta')\right) - \frac{1}{\pi(\zeta_s - \zeta')}\right\} d\zeta' + \frac{1}{4}\int_{\zeta_0}^{\zeta_{N+1}} (\zeta - \zeta')\cot\left(\pi(\zeta - \bar{\zeta}')\right) d\bar{\zeta}' \\ &- \frac{1}{4\pi}\int_{\zeta_0}^{\zeta_{N+1}} \log\left[\pi(\zeta_s - \zeta')\right] d\bar{\zeta}' - \tfrac{1}{2}\{i(\zeta - \xi_0) + K\},\end{aligned} \tag{17}$$

where

$$F(\zeta, \zeta') = (\bar{\zeta} - \bar{\zeta}')\log\left[\sin\left(\pi(\zeta - \zeta')\right)\right], \tag{18a}$$

$$G(\zeta, \zeta') = (\bar{\zeta} - \bar{\zeta}')\log\left[\pi(\zeta_s - \zeta')\right]. \tag{18b}$$

A numerical model of the nonlinear equation in the form of (17) (or of the equivalent form of (12)) was constructed as follows. On L_1 at time τ, N points representing material particles within one wavelength are defined by $\zeta_j(t) = \xi_j(t) + i\eta_j(t)$, $j = 1, \ldots, N$. The interface at τ is defined by the $N+1$ straight segments with end points (ζ_{j-1}, ζ_j), $j = 1, \ldots, N+1$. For given ζ_j the end points of integration on L_1 are defined by

$$\zeta_0 = \tfrac{1}{2}(\zeta_1 + \zeta_N - 1) \quad \text{and} \quad \zeta_{N+1} = \zeta_0 + 1.$$

The interface in one wavelength is thus completed by joining ζ_1 and ζ_N to $\zeta_N - 1$ and $\zeta_1 + 1$ (effectively in adjacent wavelengths) respectively, by straight line segments. The first two integrals in (17) cannot be evaluated analytically even along the straight segments and so were presently calculated at each τ using a simple $N+2$ point trapezoidal rule. Note that the integrand in the first integral in (17) is bounded but is not analytic at $\zeta = \zeta'$ so that some additional loss of accuracy over that associated with the trapezoidal rule is possible. The third integral was approximated by

$$\int_{\zeta_0}^{\zeta_{N+1}} \log\left[\pi(\zeta_s - \zeta')\right] d\bar{\zeta}' \simeq \sum_{j=1}^{N+1} \left(\frac{\Delta\bar{\zeta}}{\Delta\zeta}\right)_j \int_{\zeta_{j-1}}^{\zeta_j} \log\left[\pi(\zeta_s - \zeta')\right] d\zeta', \tag{19}$$

where $(\Delta\bar{\zeta}/\Delta\zeta)_j = (\bar{\zeta}_j - \bar{\zeta}_{j-1})/(\zeta_j - \zeta_{j-1})$. Each of the integrals on the right-hand side of (19) can now be evaluated analytically. With this specification (17) was applied at each of $\zeta_j, j = 1, \ldots, N$, yielding $2N$ ordinary nonlinear differential equations for $\bar{\zeta}_j$, η_j, $j = 1, \ldots, N$ which we write as

$$\frac{d\bar{\zeta}_j}{d\tau} = \Omega(\zeta_1, \zeta_2, \ldots, \zeta_N), \quad j = 1, \ldots, N, \tag{20}$$

with initial conditions $\zeta_j(0)$, $j = 1, \ldots, N$. For specified initial conditions the equations were integrated in time using an Adams predictor–corrector method in a routine due to Gear (1971). The routine varies the order of the predictor–corrector (eighth-order maximum) and the timestep $\Delta\tau$ within prescribed limits $\Delta\tau_{\min} < \Delta\tau < \Delta\tau_{\max}$ so as to keep the maxima of the error in the calculated $\zeta_j(\tau + \Delta\tau)$ (error per timestep) at less than a prescribed value E.

4. Results and discussion

A set of calculations was carried out with initial conditions defining the interface shape at $\tau = 0$ by

$$\zeta_j(0) = s_j + i\left[\frac{\delta}{\lambda} + \frac{\epsilon}{\lambda}\cos(2\pi s_j)\right], \tag{21a}$$

where

$$s_j = [j - \tfrac{1}{2}(N+1)]/N, \quad j = 1, \ldots, N. \tag{21b}$$

This presents a single cosinusoid of a wavelength λ and dimensionless amplitude ϵ/λ initially placed in $-0{\cdot}5 \leqslant \xi \leqslant 0{\cdot}5$, with equal initial spacing in the ξ direction between points. Initially $N = 40$ was chosen but, as will be seen, owing to severe contortion of the interface during some calculations, it was found that adjacent points initially close together could subsequently move rapidly apart. Hence new points were added at the mid-point of adjacent points ζ_{j-1}, ζ_j whenever these points moved such that

$$|\zeta_j - \zeta_{j-1}| > 0{\cdot}15,$$

up to a maximum determined by execution-time limitations of 60 points total on L_1.

4.1. *Results of the nonlinear calculations*

Table 1 indicates the values of δ/λ and ϵ/λ tested and also shows the corresponding values of ϵ/δ. The nondimensional period $T = -\omega t_w$ for the linear wave follows from (14) as

$$T = 4\pi(1 - e^{-4\pi\delta/\lambda})^{-1}. \tag{22}$$

Each integration started at $\tau = 0$ and was continued until either $\tau = 2T$ (calculation completed) or $\Delta\tau < \Delta\tau_{\min}$, where $\Delta\tau_{\min} = T/2000$. This last event was taken to indicate a breakdown of the calculation. The specified maximum allowable error per timestep was chosen as $E = 5 \times 10^{-4}$. Two calculations were carried out with $\epsilon/\lambda = 0$ as a check essentially of the u velocity calculation, against the known exact stationary solution $\eta = \delta/\lambda$. For these cases the maximum displacement at $\tau = 2T$ from their initial positions, of any point on the interface, was $\Delta\zeta = 0{\cdot}0006$.

All calculations with $\epsilon/\lambda = 0{\cdot}0313$ showed simple wave propagation behaviour in $0 \leqslant \tau \leqslant 2T$ as predicted by the linear theory discussed in §3.1 (see also appendix). Each of figures 2–5 shows the time evolution of the vortical interface for several

	δ/λ					
ϵ/λ	0·0625	0·125	0·250	0·500	1·000	∞
0	—	0*	—	0*	—	—
0·0313	0·5000*	0·2500*	0·1250*	0·0625*	—	0*
0·0625	—	0·5000	0·2500	0·1250	—	0
0·1250	—	—	0·5000	0·2500	0·1250	—
0·2500	—	—	—	0·5000	—	0
0·5000	—	—	—	—	0·5000	—

TABLE 1. Values of parameters for cosinusoidal initial conditions. Entries are values of ϵ/δ. * indicates that numerical solution exhibits behaviour predicted by linear theory.

selected cases with larger values of ϵ/λ. In each figure three complete wavelengths are shown but it should be noted that these are not independently evolving but are simply graphical repetitions of the basic section. For these cases, the interface behaviour is rather different to that predicted by the linear theory. Some time after $\tau = 0$ the interface minima (valleys) are found to be moving faster in the negative X direction than are the peaks. Eventually this differential movement is so large that each valley develops a tip region of very high curvature leading a lengthening re-entrant wedge or arm of irrotational fluid that is entrained into the rotational layer, moving with respect to the free stream in the negative X direction. Between these irrotational wedges and the irrotational free stream, 'lobes' or 'billows' of rotational fluid are formed.

The thickness of each wedge in each case decreases with increasing τ partly because of volume conservation (since the wedge is lengthening) and partly because the irrotational fluid velocity is slightly more positive than that of the surrounding rotational fluid so that fluid is escaping the entraining process. Much of the stretching of the boundary requiring the insertion of new points during the calculation occurs on either side of the lengthening wedge. The wedge tip was found to consist of essentially the same material particles throughout the computation, with tip velocity nearly equal to the fluid velocity that would be expected in the undisturbed parallel vortical layer at the calculated tip Y/λ position. Of the calculations illustrated only that of figure 2 extends beyond $\tau = T$. In this case the envelope of the interface shape at $\tau \simeq T$ corresponds roughly to the initial cosine shape, but with a slope discontinuity marking the entry to a, by now, collapsed irrotational wedge at the interface minimum. This suggests that the time scale for the development of nonlinear features may be taken to be of order T for given δ/λ. To investigate this hypothesis for larger ϵ/λ, the case of figure 4 ($\delta/\lambda = 0{\cdot}25$, $\epsilon/\lambda = 0{\cdot}125$) was continued by truncating the long irrotational arm at $\tau = 12{\cdot}5549$ at an arbitrary point along its length. The results are shown in figure 6. The nonlinear features continue to evolve but there is no indication of the formation of new irrotational wedges which might suggest nonlinear effects repeating every T. It seems possible, however, that with a new smooth valley forming at $\tau = 22{\cdot}8420$ further re-entrant contortions may develop for $\tau > 2T$. Unfortunately, for reasons to be discussed it was not possible to extend the calculation to these times, short of smoothing the interface shape to such an extent as to be effectively providing new cosinusoidal initial conditions, in which case wedge formation is inevitable. For

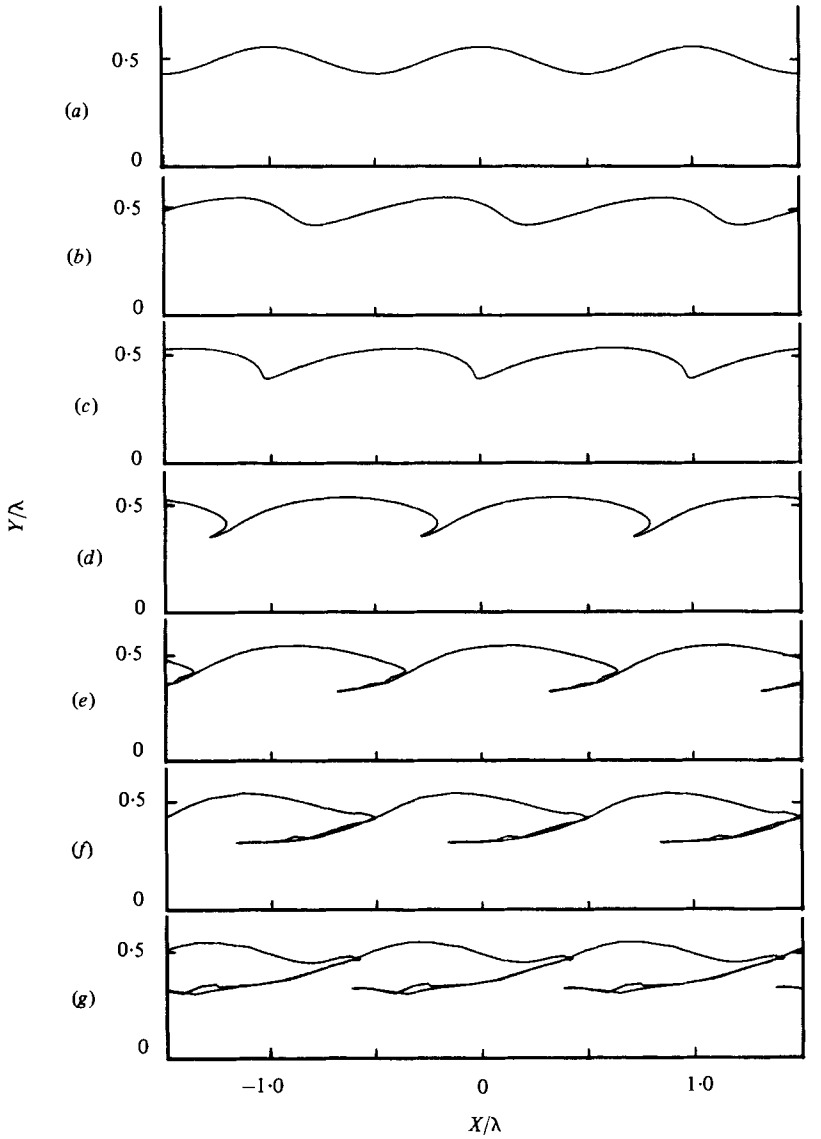

FIGURE 2. Evolution of periodic disturbance on vortical interface, $\delta/\lambda = 0{\cdot}5$, $\epsilon/\lambda = 0{\cdot}0625$, $T = 12{\cdot}5899$. (*a*) $\tau = 0$, (*b*) $\tau = 2{\cdot}5847$, (*c*) $\tau = 5{\cdot}0486$, (*d*) $\tau = 7{\cdot}5727$, (*e*) $\tau = 10{\cdot}0918$, (*f*) $\tau = 12{\cdot}6419$, (*g*) $\tau = 15{\cdot}1586$.

values of $\delta/\lambda = 1{\cdot}0, \infty$, the evolution of the interface was very similar to that for the corresponding value of ϵ/λ at $\delta/\lambda = 0{\cdot}5$. The conclusion to be drawn is that the presence of the wall has little influence on the broad shape of evolving disturbances of wavelengths $\lambda < 2\delta$ unless $\epsilon/\lambda = O(\delta/\lambda)$. It will be subsequently shown, however, that the wall presence does lead to measurable differences in the propagation speed of disturbances in this range.

In each of figures 2–6 the last frame shown represents the termination of the calculation when $\Delta\tau = \Delta\tau_{\min}$. This was usually associated with physically unrealistic

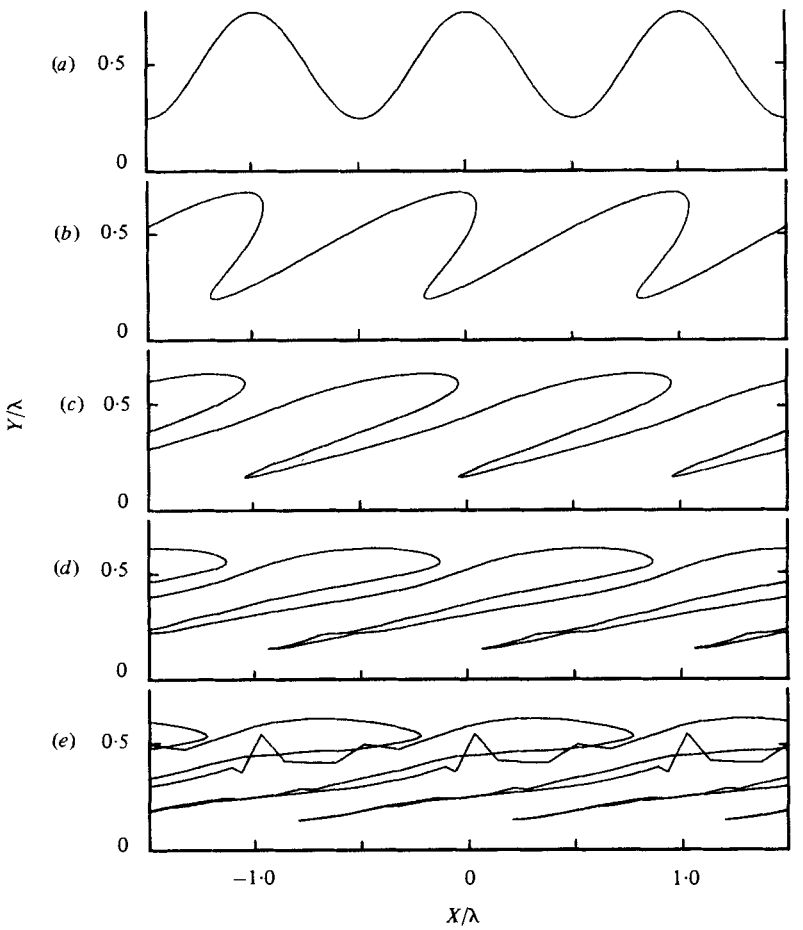

FIGURE 3. Evolution of periodic disturbance on vortical interface, $\delta/\lambda = 0{\cdot}5$, $\epsilon/\lambda = 0{\cdot}25$, $T = 12{\cdot}5899$. (*a*) $\tau = 0$, (*b*) $\tau = 2{\cdot}5274$, (*c*) $\tau = 5{\cdot}0653$, (*d*) $\tau = 7{\cdot}5756$, (*e*) $\tau = 9{\cdot}8938$.

self-intersections of the interface, for example as shown in figure 3(*e*), and also with the beginnings of significant variations from the theoretically constant value of $\lambda\delta|\omega|$, for the total circulation per wavelength. This latter quantity was monitored during the calculation and was always constant to within 1% except in these final stages. The probable reason for this breakdown of all of the calculations exhibiting nonlinear behaviour is that disturbances of wavelength $\ll \lambda$ are developing on the interface on a scale that cannot properly be resolved with the maximum of 60 interface points presently utilized. Certainly the $\delta/\lambda \to \infty$ results show that nonlinear effects may occur for infinitesimally small wavelengths for the inviscid fluid. Also, if one accepts that T given by (22) is the appropriate nonlinear inertial time scale for given δ/λ, then, since $T \to 4\pi$ for $\infty > \delta/\lambda \gtrsim 0{\cdot}25$, one might then expect that all excited scales smaller than the basic λ would develop simultaneously in a strongly coupled fashion.

To pursue this point further, several additional calculations were carried out. Several cases were treated with initial conditions given by

$$\zeta_j(0) = s_j + i[0{\cdot}250 + 0{\cdot}125\{\Delta\cos(2\pi s_j) + (1-\Delta)\cos(4\pi s_j)\}], \quad j = 1, \ldots, N, \quad (23)$$

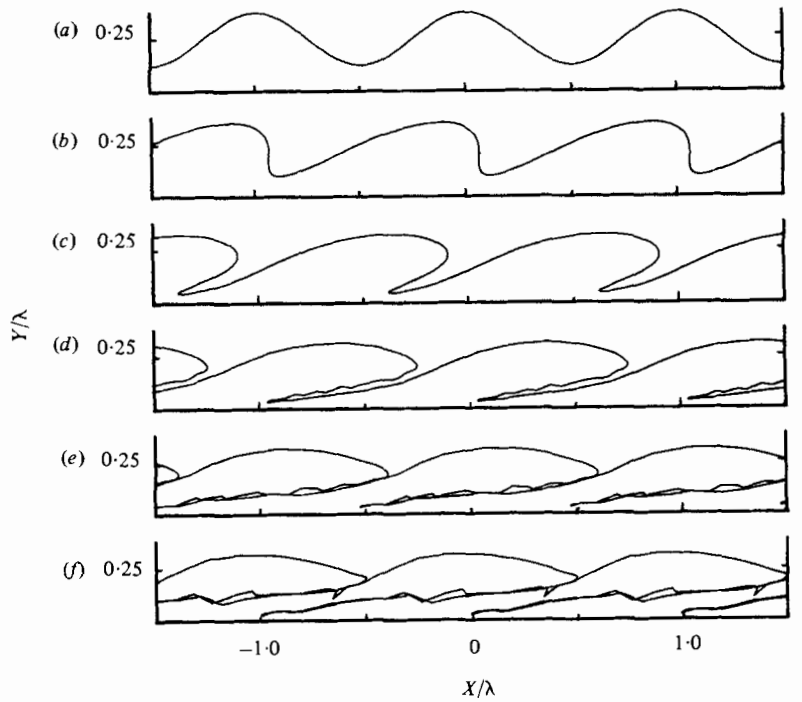

FIGURE 4. Evolution of periodic disturbance on vortical interface, $\delta/\lambda = 0{\cdot}25$, $\epsilon/\lambda = 0{\cdot}125$, $T = 13{\cdot}1339$. (*a*) $\tau = 0$, (*b*) $\tau = 2{\cdot}6995$, (*c*) $\tau = 5{\cdot}2844$, (*d*) $\tau = 7{\cdot}9140$, (*e*) $\tau = 10{\cdot}5144$, (*f*) $\tau = 12{\cdot}5549$.

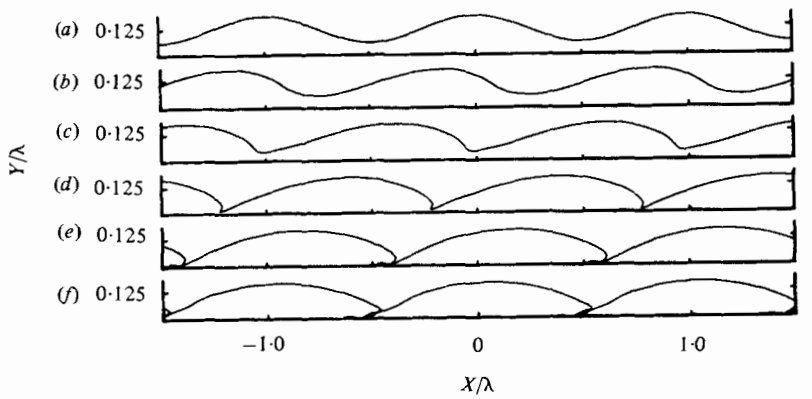

FIGURE 5. Evolution of periodic disturbance on vortical interface, $\delta/\lambda = 0{\cdot}125$, $\epsilon/\lambda = 0{\cdot}0625$, $T = 15{\cdot}8642$. (*a*) $\tau = 0$, (*b*) $\tau = 3{\cdot}1897$, (*c*) $\tau = 6{\cdot}5248$, (*d*) $\tau = 9{\cdot}5633$, (*e*) $\tau = 12{\cdot}7107$, (*f*) $\tau = 14{\cdot}3514$.

with s_j given by (21*b*). Equation (23) corresponds to a disturbance of amplitude $\epsilon/\lambda = 0{\cdot}125$ made up of fractions Δ and $1-\Delta$ respectively of two cosinusoidal modes with wavelengths 4δ and 2δ respectively. Values of $\Delta = 0{\cdot}25$, $0{\cdot}5$ and $0{\cdot}75$ were used. The results in figure 7 for $\Delta = 0{\cdot}5$ show the development of the two modes with the shorter wave mode evolving nonlinearly while being carried on the back of the rotational lobe corresponding to the longer wavelength. For $\Delta = 0{\cdot}25$, $0{\cdot}75$ the shorter

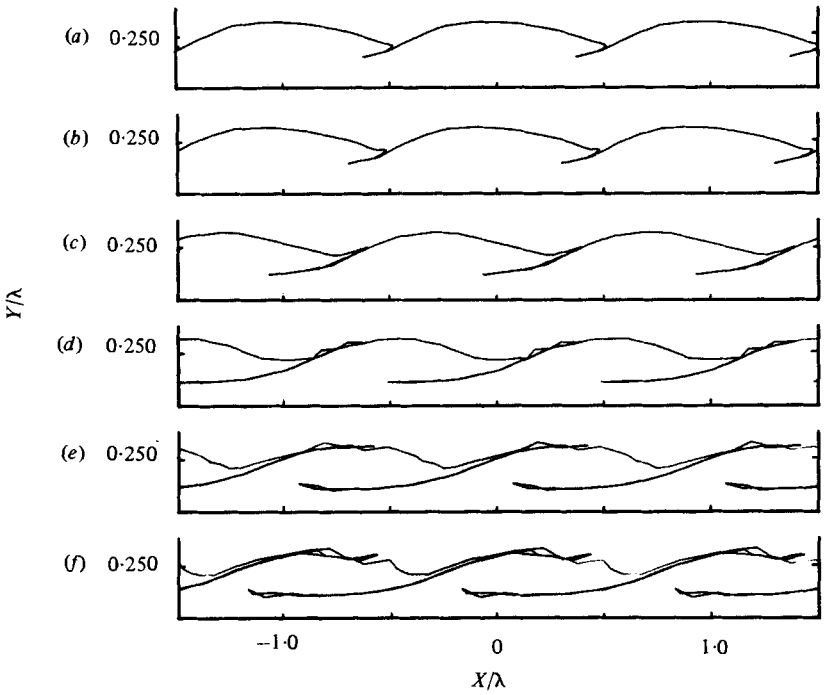

FIGURE 6. Continuation of calculation of figure 4, $\delta/\lambda = 0{\cdot}25$, $\epsilon/\lambda = 0{\cdot}125$. (*a*) $\tau = 12{\cdot}5549$, (*b*) $\tau = 13{\cdot}1661$, (*c*) $\tau = 15{\cdot}2935$, (*d*) $\tau = 18{\cdot}4297$, (*e*) $\tau = 20{\cdot}9665$, (*f*) $\tau = 22{\cdot}8420$.

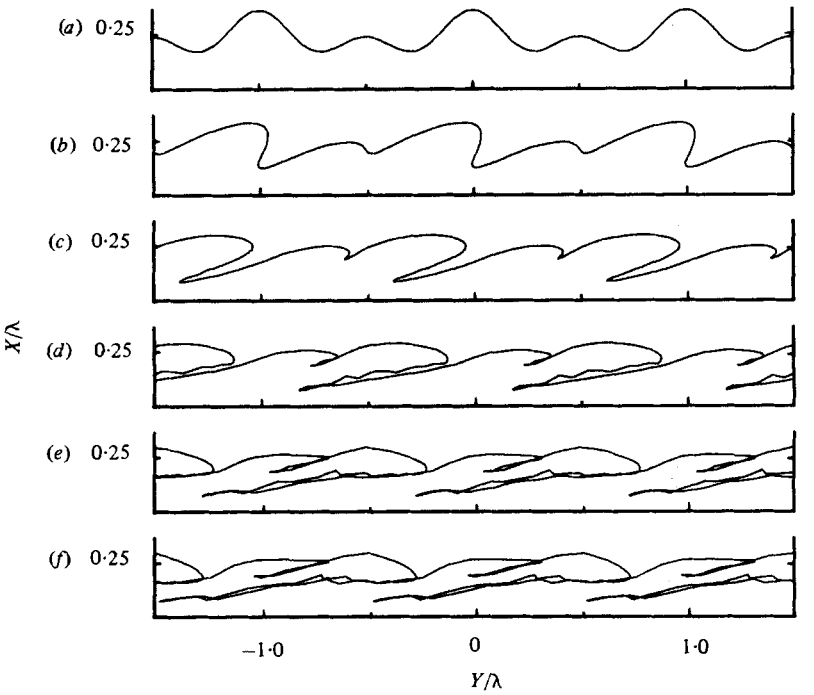

FIGURE 7. Evolution of periodic disturbance on vortical interface; two-mode interaction, $\delta/\lambda = 0{\cdot}250$, $\epsilon/\lambda = 0{\cdot}125$, $\Delta = 0{\cdot}5$. (*a*) $\tau = 0$, (*b*) $\tau = 2{\cdot}7232$, (*c*) $\tau = 5{\cdot}2829$, (*d*) $\tau = 7{\cdot}8935$, (*e*) $\tau = 10{\cdot}5150$, (*f*) $\tau = 11{\cdot}6506$.

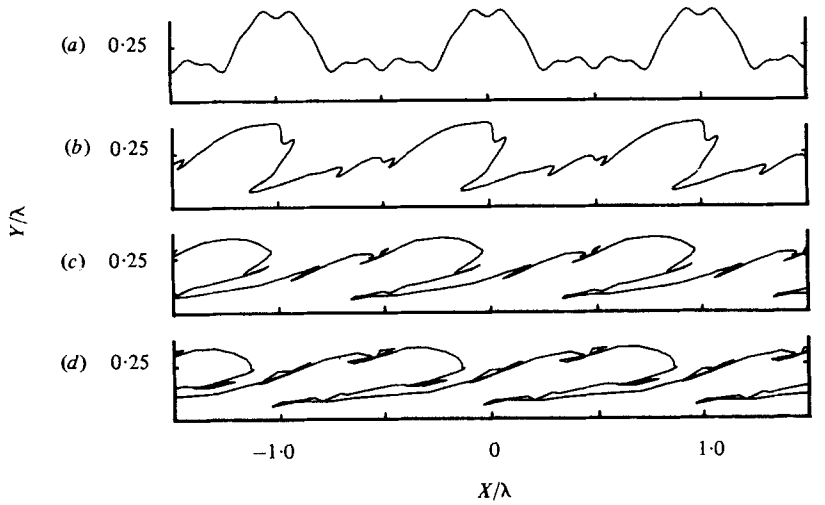

FIGURE 8. Evolution of disturbance on vortical interface; four-mode interaction, $\delta/\lambda = 0{\cdot}25$. (*a*) $\tau = 0$, (*b*) $\tau = 2{\cdot}6307$, (*c*) $\tau = 5{\cdot}2717$, (*d*) $\tau = 7{\cdot}2270$.

and longer wavelength respectively is dominant with results similar to these of figures 3 and 4 respectively. Finally a case with initial conditions given by

$$\zeta_j(0) = s_j + i[0{\cdot}250 + 0{\cdot}125\cos(2\pi s_j) + 0{\cdot}0625\cos(4\pi s_j) - 0{\cdot}0312\cos(8\pi s_j) - 0{\cdot}0156\cos(16\pi s_j)], \quad j = 1, \ldots, N, \quad (24)$$

was tested with $N = 56$ initially, corresponding to four modes of progressively smaller wavelengths with amplitudes chosen so that $\epsilon/\lambda = 0{\cdot}125$ for each mode. As shown in figure 8 the calculation does not last for a very long fraction of T since the smaller-scale disturbances soon develop their own nonlinear convolutions leading to a very complicated boundary or interfacial shape and to subsequent breakdown of the calculation.

4.2. *Discussion*

Spacially non-uniform distortion of convecting free vortical boundaries have been noted by several workers. Deem & Zabusky (1978*b*) and Seo *et al.* (1979) found that the timewise evolution of a finite perturbation to the shape of a uniform circular vortex eventually led to the formation of an interfacial cusp and subsequently to the appearance of a filament of detrained vorticity projecting into the irrotational fluid. Similar phenomena were found to result from the mutually interactive distortion of groups of initially circular vortices. Moffatt & Moore (1979) have shown that the response of a Hills spherical vortex to an axisymmetric disturbance is to either entrain/detrain a narrow spike of irrotational/rotational fluid into/out-of the vortex at the rear stagnation point. The type of motion which occurs depends on the geometry of the perturbation. Moffatt & Moore interpret this behaviour as due to the presence of a rear stagnation point near which the disturbed irrotational flow quickly deforms the initial perturbed boundary shape.

For the present configuration a related physical explanation is suggested as follows: for sufficiently large ϵ/λ, the interfacial valleys will reach the vicinity of the fluid critical layer, defined as that Y station at which the timewise mean X fluid velocity is equal to the linearized wave speed c. At larger ϵ/λ, deeper into the vortical layer, it

may be thus expected that the mean flow would tend to convect material particles on the interfacial valleys in the negative X direction with speeds exceeding $|c|$, leading then to differential wave crest/valley movement and to the onset of nonlinearity. In this sense the nonlinear interface behaviour may be viewed as essentially kinematic, i.e. the spacially non-uniform distortion of a mode of a neutrally stable, dispersive Kelvin–Helmholtz wave by the mean flow at or below the fluid critical layer. Thus the critical layer here plays the same role as does the rear stagnation point in the spherical vortex flow. There is an important difference, however, in that the spherical vortex distortion may be generated by an infinitesimal perturbation, whereas in the present case a finite-amplitude wave is evidently required.

Given the above, an estimate for the range of validity of the linear theory follows by supposing that the unperturbed fluid speed at the Y position of the interface valley must not exceed c. Using (13), one obtains

$$\frac{\epsilon}{\lambda} < \frac{1}{4\pi}(1 - e^{-4\pi\delta/\lambda}). \tag{25}$$

For $\delta/\lambda \lesssim 0{\cdot}5$ this leads to $\epsilon/\lambda < 1/4\pi$, which as a rough estimate is consistent with the present results. For long waves the result is $\epsilon/\lambda < \delta/\lambda$, which must always be true, so that we might expect that the linear theory is uniformly valid in ϵ/λ in this limit.

Several studies of the outer-intermittent region of the constant-pressure turbulent boundary layer have revealed features on the scale of the layer thickness which distinctly resemble those seen in the present calculations. Falco (1977), using a smoke-marking flow-visualization technique, observed large-scale motions 'defined by the bulge at the top of the layer and by concentration gradients that extend from the smoke–no-smoke interface deep into the layer'. The average distance between bulges was found to be about 2·5 times the nominal boundary-layer thickness (that point at which $u = 0{\cdot}99U_0$) which we may here identify with δ. A combination of measurements from hot wires arrayed across the boundary layer and from wall shear-stress probes led Brown & Thomas (1977) to suggest the existence of a coherent large-scale structure in the outer part of the boundary layer of length about 2δ and tilted forward in the upstream direction at an angle of about 18–20° to the wall. This angle is very nearly that marked by smoke concentration gradients in Falco's photographs and is not too different from the inclination angle of the irrotational arms in the present calculations (see figures 2–6), while they remain of finite thickness. In their recent smoke-marking flow-visualization studies Head & Bandyopadhyay (1981) also note the presence of a feature associated with low smoke concentration and inclined at about 20° to the wall. They do not regard this as part of a large coherent eddy, however, but rather as a random alignment of the tops of hairpin-like vortices originating from the viscous sublayer and projecting into the outer part of the boundary layer at an angle of about 45°. Head & Bandyopadhyay do not consider that any coherent large-scale motion is present in the outer reaches of the layer other than a slow overturning motion.

But, whether or not they constitute part of a recognizably coherent motion, there seems little doubt that bulges or lobes of turbulent fluid can be identified at the rotational–irrotational fluid interface and that these bulges move slightly slower than the free stream relative to an observer stationary with respect to the wall. Estimates of the convection velocity at the front or crest of and at the rear or back of these bulges were deduced by Kovasznay *et al.* (1970) from space–time velocity correlation

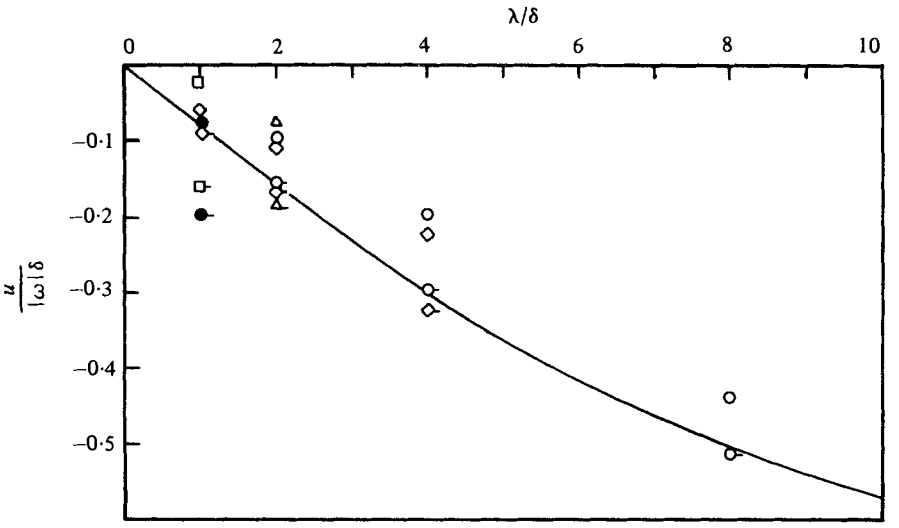

FIGURE 9. Calculated lobe front and back velocities against λ/δ. ○, $\epsilon/\lambda = 0{\cdot}0625$; □, $\epsilon/\lambda = 0{\cdot}125$; △, $\epsilon/\lambda = 0{\cdot}25$; ⊡, $\epsilon/\lambda = 0{\cdot}5$; ●, measurement, Kovasznay *et al.* (1970). Flagged symbols represent lobe back velocities. ——, linearized wave velocity.

measurements. These are compared in figure 9 with estimates of the lobe front and back velocities obtained from the present results. The calculated lobe front velocities were taken as the mean velocity at the upstream point of infinite slope $d\eta/d\xi$, while the back velocities were taken as the average velocity on the lobe back at $\eta = \delta/\lambda$. To enable comparison with experiment, estimates of the experimental ω and λ are required. Kovasznay *et al.* found that the nearly constant value of ω within the turbulent fluid near the bulges was given by $|\omega|\delta \simeq 8{\cdot}3u_*$, where $u_* = (\tau_w/\rho)^{\frac{1}{2}}$ is the friction velocity, τ_w is the wall shear stress and ρ is the fluid density. For their experiment $u_*/U_0 \simeq 0{\cdot}045$ giving $|\omega|\delta \simeq 0{\cdot}37U_0$. The effective experimental λ has been taken as the mean of the characteristic bulge streamwise dimension of order δ given by Kovasznay *et al.* The data are at least consistent with the trend of the theory in figure 9 even though the latter show sizeable variation with ϵ/λ at $\delta/\lambda = 1{\cdot}0$. Given that the measurements themselves show considerable variation across the outer part of the layer as shown in figure 16 of Kovasznay *et al.*'s paper (the quoted values are averages), the comparison with the predicted results is regarded as encouraging. Figure 10 shows calculated instantaneous streamline patterns for the case $\delta/\lambda = 0{\cdot}250$, $\epsilon/\lambda = 0{\cdot}125$, as seen in a framework moving with the average lobe velocity of $-0{\cdot}27|\omega|\delta$. In figure 10(*b*), the general pattern of the motion within the lobe is circulatory, being upwards and away from the wall along the lobe back, and towards the wall at the lobe front. A saddle point (moving stagnation point) may be seen near to but not actually on the lobe back near the mouth of the arm of irrotational fluid. The pattern depicted in figure 10(*b*) is characteristic of streamline patterns obtained for other cases and is generally similar to the pattern of motion within the large-scale bulges observed by Kovasznay *et al.* (1970), Falco (1977) and Brown & Thomas (1977).

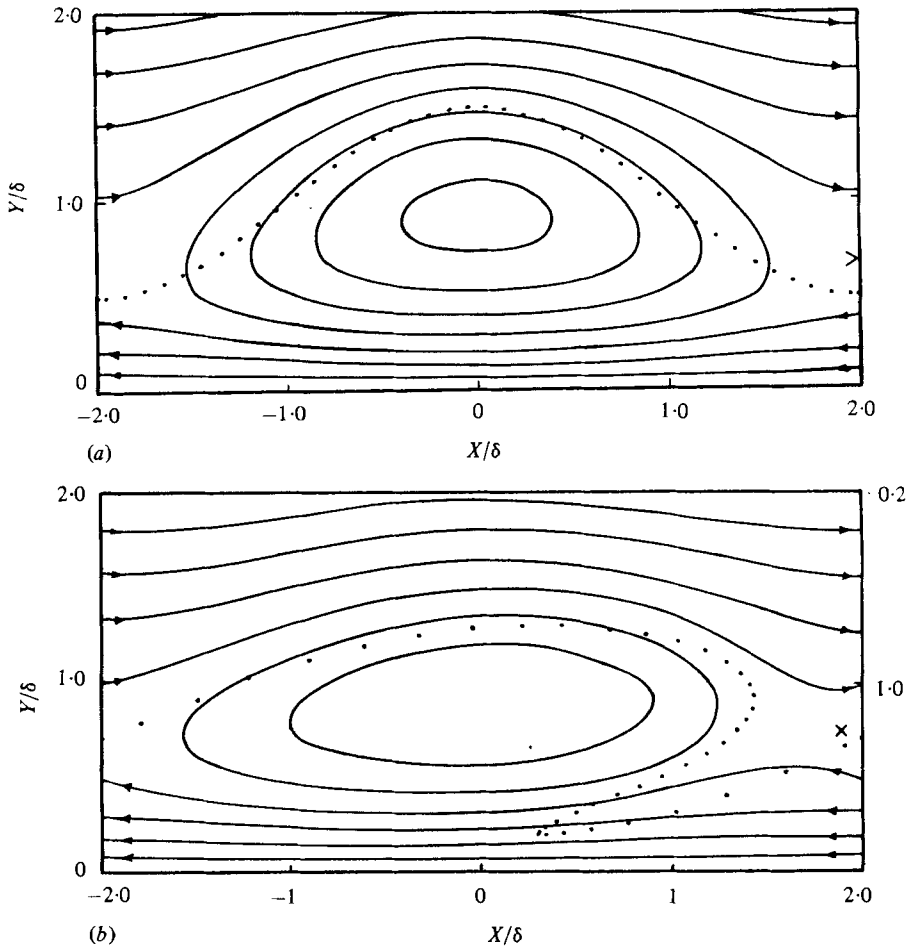

FIGURE 10. Instantaneous streamlines as seen moving in reference frame with velocity $-0{\cdot}27|\omega|\delta$ relative to free stream, $\delta/\lambda = 0{\cdot}25$, $\epsilon/\lambda = 0{\cdot}125$. ——, streamlines; ..., points on vortical interface. (*a*) $\tau = 0$, interior streamline $\Psi'/|\omega|\delta^2 = -0{\cdot}350$, (*b*) $\tau = 5{\cdot}2844$, interior streamline $\Psi'/|\omega|\delta^2 = -0{\cdot}300$, streamline spacing $\Delta\Psi'/|\omega|\delta^2 = -0{\cdot}05$; ×, approximate position of saddle point.

5. Conclusions

The present results show that the nonlinear behaviour of the constant-vorticity layer may be very different from the neutral stability predicted by the linear theory. For a finite initial disturbance, nonlinearity is evidently possible on all wavelengths from effectively zero (for the inviscid fluid) to those very long compared to the layer thickness, where it is attenuated only by limitations to the allowable size of disturbance amplitudes imposed by the presence of the wall. There is sufficient similarity of our results to existing observations of motions in the outer part of the boundary layer to suggest that the two-dimensional spacially non-uniform entrainment mechanism discussed in §4.2 may play a significant role in the outer-layer behaviour. Three-dimensional motions in the layer may be produced either by the hairpin-like vortices of Head & Bandyopadhyay (1981), originating through events in the viscous sublayer

and projecting outwards, or by spanwise buckling of vortex lines associated with the mean shear in the outer part of the layer, or by a combination of both effects. At sufficiently high Reynolds numbers, the vortex lines associated with the three-dimensional motion probably point both towards and away from the wall so that this motion might be thought of as being generated by a dipole field tilted at 45° to the wall in the direction of the mean flow (Perry 1979, private communication). One possible explanation for the similarity of the present two-dimensional results and the outer-boundary-layer behaviour is that such a dipole field induces slow three-dimensional distortions of the lobe-like rotational structures generated by the nonlinear vortical interaction associated with mean shear but does not otherwise exert significant dynamical influence on this interaction. Alternatively a three-dimensional instability may in fact be required to generate a local disturbance of sufficient amplitude to initiate critical-layer interfacial distortion associated with mean shear.

In contrast to the behaviour of the free shear layer the wall layer exhibits no preference for any particular scale or wavelength. The inviscid free shear layer of thickness δ is known to be linearly stable to two-dimensional disturbances of wavelength $\lambda < 5\delta$ (Rayleigh 1880) and unstable otherwise with maximum temporal amplification occurring at λ about 7δ to 8δ (Rayleigh 1880; Michalke 1964). Thus for wavelengths of this order very strong nonlinear instabilities leading to the roll-up and pairing phenomena observed in mixing and free shear-layer experiments and simulated numerically by Acton (1976) occur, which are readily identified with notions of coherent large eddies. Smaller-scale nonlinearities such as those seen here may develop on and be convected with the large-scale motion but the overall dynamics of the flow are clearly dominated by the larger structures. In the wall layer a disturbance of any wavelength locally of sufficient amplitude in the sense of (25) may develop spacially non-uniform features leading then to a broad spectrum of possible active eddy scales. Thus, if our results are relevant to the behaviour of the outer part of the turbulent boundary layer, it must be concluded that they neither support nor contradict the large-scale motions hypothesis since in each individual calculation a definite periodic wavelength was imposed, which necessarily leads to ordered motion on this scale, but no preferential wavelength was indicated. The present results may, however, indicate the form such motions would take if indeed they are present. Of course, the possibility remains that some dominant scaling is provided through the coupling of events occurring in the region of the viscous sublayer and the outer part of the layer (responding perhaps through the mechanism described here) as part of an as yet imperfectly understood process occurring in the boundary layer as a whole.

Finally a comment is necessary on the use of (21) with finite ϵ/λ, as the initial condition for the calculations. A referee has pointed out that this initial condition is somewhat artificial since, in view of the stability of the flow to small perturbations, there is no reason at all to expect to find such finite-amplitude waves on the interface. We accept that this may be seen to represent a conceptual difficulty in the context of the two-dimensional motion. We can then only justify the use of (21) (with finite ϵ/λ) firstly on the grounds of the rather surprising and unexpected response of the vortical layer and secondly on the suggested relevance of this response to the outer turbulent boundary-layer flow.

Appendix. Solution of the linearized equation

Here we consider the evolution of small perturbations to the undistributed shape of the vortical interface. For this purpose, rather than utilizing the Lagrangian description implicit in (11) it is more convenient to work within an Eulerian specification, describing the displacement of the interface at given X by

$$y(X,t), \quad \tfrac{1}{2}\lambda \geqslant X \geqslant -\tfrac{1}{2}\lambda.$$

The equation of $y(X,t)$ may be written as

$$\left(\frac{\partial y}{\partial t}\right)_X = v - u\left(\frac{\partial y}{\partial X}\right)_t, \tag{A 1}$$

where $u - iv$ is given by the right-hand side of (11) with $z = X + iy(X,t)$. The linearized analysis proceeds by writing

$$\left.\begin{aligned} y(X,t) &= y_0(X,t) + \epsilon' y_1(X,t) + \ldots, \\ u(X,t) &= u_0(X,t) + \epsilon' u_1(X,t) + \ldots, \\ v(X,t) &= v_0(X,t) + \epsilon' v_1(X,t) + \ldots, \\ dz &= dX + i\epsilon'\left(\frac{\partial y_1}{\partial X}\right)_t dX + \ldots, \end{aligned}\right\} \tag{A 2}$$

where $y_0(X,t) = \delta$, $u_0(X,t) = v_0(X,t) = 0$ are the unperturbed state of the vortical interface and ϵ' is a small parameter. Substituting (A 2) into the right-hand side of (11), the result into (A 1), expanding in ϵ' and retaining terms linear in this quantity, one obtains the linearized equation for $y_1(X,t)$

$$\frac{\partial y_1(X,t)}{\partial t} = \frac{\omega}{2\lambda} \int_{-\lambda/2}^{\lambda/2} y_1(X',t)\, \mathrm{Re}\left\{\cot\left[\frac{\pi}{\lambda}(X - X')\right] - \cot\left[\frac{\pi}{\lambda}(X - X' + 2i\delta)\right]\right\} dX', \tag{A 3}$$

where the first term on the right-hand side represents a Cauchy principal-value integral.

We seek a solution to (A 3) of the form

$$y_1(X,t) = a_1(t)\cos\left(\frac{2\pi X}{\lambda}\right) + a_2(t)\sin\left(\frac{2\pi X}{\lambda}\right), \tag{A 4}$$

where $a_1(t)$, $a_2(t)$ are amplitude functions to be determined. Substituting (A 4) into (A 3) and carrying out the integrations on the right-hand side yields

$$\frac{da_1}{dt} = -Ja_2, \quad \frac{da_2}{dt} = Ja_1, \tag{A 5}$$

where $J = \frac{1}{2}\omega(1 - e^{-4\pi\delta/\lambda})$. This is sufficient to indicate neutral stability. Solving (A 5) for initial conditions $a_1(0)$, $a_2(0)$ leads to the solution

$$y_1(X,t) = a_1(0)\cos\left[\frac{2\pi}{\lambda}(X - ct)\right] + a_2(0)\sin\left[\frac{2\pi}{\lambda}(X - ct)\right], \tag{A 6}$$

representing a neutrally stable dispersive wave travelling in the same direction relative to the fluid at infinity as is the wall with velocity

$$c = \frac{\omega\lambda}{4\pi}(1 - e^{-4\pi\delta/\lambda}). \tag{A 7}$$

REFERENCES

ACTON, E. 1976 *J. Fluid Mech.* **76**, 561–592.

BATCHELOR, G. K. 1967 *An Introduction to Fluid Dynamics.* Cambridge University Press.

BERK, H. L., NIELSEN, C. E. & ROBERTS, K. V. 1970 *Phys. Fluids* **13**, 980–995.

BIRKHOFF, G. 1962 *Proc. Symp. Appl. Math. Am. Math. Soc.* **13**, 55–76.

BROWN, G. L. & THOMAS, A. S. W. 1977 *Phys. Fluids Suppl.* **20**, 243–252.

CHRISTIANSEN, J. P. 1973 *J. Comput. Phys.* **13**, 363–379.

CHRISTIANSEN, J. P. & ZABUSKY, N. J. 1973 *J. Fluid Mech.* **61**, 219–243.

DEEM, G. S. & ZABUSKY, N. J. 1978*a* *Phys. Rev. Lett.* **40**, 859–862.

DEEM, G. S. & ZABUSKY, N. J. 1978*b* In *Solitons in Action* (ed. K. Lonngren & A. Scott), pp. 277–293. Academic.

FALCO, R. E. 1977 *Phys. Fluids Suppl.* **20**, 124–132.

FINK, P. T. & SOH, W. K. 1978 *Proc. Roy. Soc.* A **362**, 195–209.

GEAR, C. W. 1971 *Numerical Initial Value Problems in Ordinary Differential Equations.* Prentice Hall.

HEAD, M. R. & BANDYOPADHYAY, P. 1981 *J. Fluid Mech.* (to appear).

KOVASZNAY, L. S. G., KIBENS, V. & BLACKWELDER, R. F. 1970 *J. Fluid Mech.* **41**, 283–325.

LEONARD, A. 1980 In *Turbulent Shear Flows II* (ed. L. J. S. Bradbury), pp. 67–77. Springer.

MICHALKE, A. 1964 *J. Fluid Mech.* **19**, 543–556.

MOFFATT, H. K. & MOORE, D. W. 1979 *J. Fluid Mech.* **87**, 749–760.

MOORE, D. W. 1978 *Stud. App. Math.* **58**, 119–140.

MOORE, D. W. 1979 *Proc. Roy. Soc.* A **365**, 105–119.

PERRY, A. E. & FAIRLIE, B. D. 1975 *J. Fluid Mech.* **69**, 657–672.

PERRY, A. E., LIM, T. T. & CHONG, M. S. 1980 *A.I.A.A. paper* 80-1358.

RAYLEIGH, LORD 1880 *Scientific Papers*, vol. 1, pp. 474–487. Also *Proc. Lond. Math. Soc.* **11**, 57–80.

RAYLEIGH, LORD 1887 *Scientific Papers*, vol. 3, pp. 17–23. Also *Proc. Lond. Math. Soc.* **19**, 67–74.

ROBERTS, K. V. & CHRISTIANSEN, J. P. 1972 *Comput. Phys. Commun. Suppl.* **3**, 14–32.

ROTT, N. 1956 *J. Fluid Mech.* **1**, 111–128.

SAFFMAN, P. G. & BAKER, G. R. 1979 *Ann. Rev. Fluid. Mech.* **11**, 95–122.

SEO, R. L., JOYNT, R. C. & LLEWELYN, R. P. 1979 State Electricity Commission of Victoria unpub. rep.

ZABUSKY, N. J., HUGHES, M. H. & ROBERTS, K. V. 1979 *J. Comp. Phys.* **30**, 96–106.